Solar Energy Materials and Solar Cells 186 (2018) 227–235

Contents lists available at ScienceDirect

Solar Energy Materials and Solar Cells

journal homepage: www.elsevier.com/locate/solmat

Nanocomposite $(CuS)_x(ZnS)_{1-x}$ thin film back contact for CdTe solar cells: Toward a bifacial device

Kamala Khanal Subedi, Ebin Bastola, Indra Subedi, Zhaoning Song, Khagendra P. Bhandari, Adam B. Phillips, Nikolas J. Podraza, Michael J. Heben, Randy J. Ellingson*

Wright Center for Photovoltaics Innovation and Commercialization, Department of Physics and Astronomy, The University of Toledo, Toledo, OH 43606, USA

ARTICLE INFO

Keywords:
$(CuS)_x(ZnS)_{1-x}$
CdTe solar cells
Back contact
Bifacial
Chemical bath deposition
Nanocomposite thin film

ABSTRACT

Critical avenues to increase energy yield for CdTe photovoltaic (PV) technology, such as bifacial cells or tandem cells designs, rely on the need to develop transparent back contact approaches that enable high efficiency and high transparency. We report the properties of earth-abundant p-type transparent conducting nanocomposite (NC) thin film $(CuS)_x(ZnS)_{1-x}$, deposited by low-cost chemical bath deposition method. Nanocomposite films of ~ 45 nm thickness transmit > 70% of the visible light and show compact grains of size ~ 10 nm. We investigate the photovoltaic performance of both opaque and semi-transparent CdTe solar cells using $(CuS)_x(ZnS)_{1-x}$ NC thin films as a back contact interface layer. Introduction of the NC layer between the CdTe and a standard Cu/Au metallization process yielded the best device efficiency of 13%, representing a 3.2% relative improvement over the standard Cu/Au back contact. Semi-transparent CdTe devices finished with an indium tin oxide (ITO) layer allowed for comparison of front and back illumination schemes. Experimental and modeling results confirm that the bifacial device configuration leads to significant recombination losses under back illumination due to the absence of a charge separating field, a relatively high interface recombination rate, and an insufficient electron diffusion length. Once optimized, and with an improved interface and bulk CdTe carrier lifetimes, this NC earth-abundant transparent conductor based on Cu, Zn, and S may serve as an effective, inexpensive, low-toxicity back contact layer for a bifacial CdTe solar cell.

1. Introduction

Cadmium telluride (CdTe) remains the leader as measured by the shortest energy payback time and, correspondingly, the largest energy return on energy invested [1,2]. CdTe has closed the module-level efficiency gap with multi-crystalline silicon [3]. The recent increases in the minority carrier lifetime and diffusion length have brought closer the possibility to increase photovoltaic (PV) energy generation by using a bifacial module architecture. In addition, the semitransparent solar cell holds novel application like building integrated PV [4]. Bifacial solar cells were first fabricated in 1978 by the Luque et al. [5], more recently Tiwari et al. have utilized indium tin oxide (ITO) as a transparent back contact layer to CdTe solar cells [6], and Khanal et al. used transparent single wall carbon nanotubes for bifacial CdTe solar cells [7]. Bifacial solar cells allow for the conversion of sunlight incident from either or both sides of the device, allowing for the opportunities of higher total conversion efficiency and higher energy yield under typical operating conditions [8–10]. Thin film CdTe solar cells have long been identified as a cost-effective solution for utility-scale photovoltaic systems, and the development of an efficient bifacial architecture would provide an additional advantage to the already low cost per Watt of the technology.

The fabrication of efficient CdTe solar cells involves different steps including fabrication of the front window layer, deposition of CdTe thin film, and back contact processing. Following CdTe thin film deposition, treatment with cadmium chloride ($CdCl_2$) enhances grain growth, while yielding CdS/CdTe layer interdiffusion, and improvements to the electronic properties and photovoltaic performance in the finished CdTe solar cells [11,12]. In case of back contact processing, a highly-transparent back contact enables CdTe top cell tandem photovoltaic designs [13,14]. Nonetheless, highly effective transparent back contacts designed for p-CdTe remain challenging due to a dearth of p-type metal oxides, and to the simultaneous need to passivate against interface recombination losses. In addition, the deep work function of ~ 5.7 eV exhibited by CdTe presents a challenge for creating a low resistance and barrier-free back contact for use in the CdS/CdTe solar cells [15–18]. In analogy with their more prevalent n-type counterparts, p-type transparent conductors ideally exhibit high values of free hole concentration,

* Corresponding author.
E-mail address: Randy.Ellingson@utoledo.edu (R.J. Ellingson).

https://doi.org/10.1016/j.solmat.2018.06.025
Received 26 April 2018; Received in revised form 7 June 2018; Accepted 13 June 2018

optical transparency, and electrical conductivity [19,20]. Numerous materials have demonstrated varying levels of performance as the CdTe back contact interface layer, including but not limited to Cu/Au [21], RF-magnetron sputtered Cu-doped ZnTe [22], thermally evaporated Cu_2Te [23], solution-processed pure and alloyed iron pyrite nanocrystals [24,25], and single-walled carbon nanotubes [26]. In each of these cases, a Schottky barrier forms at the rear interface due to CdTe's deep valence band and work function [27,28]. First Solar has implemented the p-type ZnTe:Cu back contact [29]. ZnTe has a suitably deep valence band edge which together with the 2.24 eV band gap energy places the conduction band edge sufficiently shallow as to efficiently reflect electrons away from the back contact interface, which aids in reducing recombination at the back contact [30]. None of the above mentioned back contacts serve as a transparent back-contact electrode, which is needed for the high efficiency bifacial solar cells.

$(CuS)_x(ZnS)_{1-x}$ nanocomposite (NC) can be used as a transparent hole transport layer (HTL), or buffer layer, at the interface between CdTe and a metallization layer (which may also be transparent as in case of ITO). The back-illuminated performance demonstrated here using $(CuS)_x(ZnS)_{1-x}$ as an HTL, together with solar cell capacitance simulator (SCAPS) modeling with improved absorber layer properties, shows that as the CdTe continues to improve, bifacial cells will very likely show economic benefits [31]. Previously, the Cu doping process has been reported to modify the microstructure and optoelectronic properties of ZnO [32]. Highly Cu doped NC thin films consisting of p-type $(CuS)_x(ZnS)_{1-x}$ have shown high visible light optical transparency with a free hole concentration of $\sim 10^{21}$ cm^{-3} supporting high electrical conductivity [33]. The back contact barrier height in CdTe thin films can be minimized by inserting a thin semiconductor layer with very high carrier density [34] or by increasing the conductivity of the CdTe layer. However, doping of polycrystalline CdTe is not straightforward due to the tendency to self-compensate. The p-type $(CuS)_x(ZnS)_{1-x}$ with its high carrier density forms a shallow barrier with a back contact metal so that photo-generated holes can easily propagate to the back contact metals with reduced potential loss [18,35]. Many efforts have been reported toward developing effective hole-selective contacts to CdTe polycrystalline solar cells, and this class of p-type NC thin film offers several attractive properties for such an application. P-type $(CuS)_x(ZnS)_{1-x}$ has been deposited by numerous methods – such as chemical bath deposition (CBD) [36], electrochemical deposition [37], and pulsed laser deposition [38], and has been demonstrated as a contact material for amorphous-Si passivated monocrystalline Si solar cells [33]. Ma et al. used the CBD technique to deposit Zn doped CdS to increase the transmittance of the CdS film [39]. Here, we have employed the CBD method to deposit a thin layer of $(CuS)_x(ZnS)_{1-x}$ on CdTe PV devices [40–42]. The solution-based CBD technique enables controlled deposition of a thin film onto a substrate immersed in a dilute solution of precursors. While the CBD film can be formed either via ion-by-ion or cluster–by-cluster processes [43], our method suppresses the cluster-by-cluster mechanism to form high quality NC films [44].

Here, we report the fabrication of $(CuS)_x(ZnS)_{1-x}$ thin films, characterization, and the observed performance when used as the HTL in CdTe devices. The $(CuS)_x(ZnS)_{1-x}$ thin films were characterized using scanning electron microscopy (SEM), X-ray diffraction (XRD), UV–Vis–NIR spectrophotometry, and spectroscopic ellipsometry (SE). Thin films ($\sim$ 45 nm thick) show > 70% visible spectral range transparency. Our study shows that these films are highly conductive with a carrier density of $\sim 10^{21}$ cm^{-3}, making them promising hole transport materials for CdTe solar cells. Using $(CuS)_x(ZnS)_{1-x}$ NC as hole transport materials in CdTe devices, the best device efficiency (η) of > 13%, and a fill factor (FF) > 73% have been observed. In addition, we discuss experimental and simulation results for illuminating these CdTe devices, when finished with ITO, through the p-type back contact.

2. Experimental details

2.1. Chemicals

Copper (II) sulphate ($CuSO_4$, 99%) zinc acetate ($Zn(CH_3COO)_2$, 99.9%), thioacetamide (C_2H_5NS, 99%), and edetate disodium salt dihydrate (Na_2EDTA, 99%) were purchased from Alfa Aesar. All chemicals were stored at room temperature and used without further purification.

2.2. Film preparation

Glass substrates were ultrasonically cleaned using detergent and deionized water (DIW) for 30 min, rinsed several times with DIW, cleaned in methanol for 15 min, rinsed again by acetone and finally by DIW before drying the substrate using dry N_2 in air. The $(CuS)_x(ZnS)_{1-x}$ thin films were fabricated using a procedure reported previously [33,36]. Three solutions were prepared to fabricate $x = 0.64$ and $x = 0.8$: (1) with total concentration of 0.1 M of $CuSO_4$ and $Zn(CH_3COO)_2$ in 50 mL DIW; (2) 0.1 M concentration of C_2H_5NS in 50 mL DIW, and (3) 0.1 M concentration of Na_2EDTA in 25 mL DIW, with total 125 mL solution. The concentration of $CuSO_4$ and $Zn(CH_3COO)_2$ can be varied to produce different x in $(CuS)_x(ZnS)_{1-x}$. $Zn(CH_3COO)_2$ molarity is dominated by the $CuSO_4$ because the solubility product of CuS is much lower than ZnS [45]. The solution 1 and solution 3 were mixed thoroughly in an ultrasonic bath for 20 min at a temperature of 30 °C and subsequently mixed together with solution 2. The cleaned substrate was immediately placed vertically inside the solution and the beaker was covered with aluminum foil to prevent evaporation. The mixed solution was placed on the water bath maintaining the temperature at 80 °C with continuous stirring. The film growth reaction continued for 55 min. The substrate coated with the NC film was removed from the solution, washed with DIW, and dried by N_2 in the air.

2.3. Film characterization

A Hitachi S-4800 UHR scanning electron microscope (SEM) was used to study the surface morphology of $(CuS)_x(ZnS)_{1-x}$ films. Energy dispersive x-ray spectroscopy (EDS) integrated into the Hitachi SEM instrument operating at 20 kV and 15 μA was used to investigate the composition of the $(CuS)_x(ZnS)_{1-x}$ films. The sheet resistance was measured using the Lucas four-point probe. The XRD patterns were taken by a Rigaku Ultima III X-ray Diffractometer at 40 kV accelerating voltage and 44 mA currents. Unpolarized transmittance and reflectance spectra were measured by a PerkinElmer Lambda 1050 UV/Vis/NIR spectrophotometer. Room temperature ellipsometric spectra (in $N = \cos 2\Psi$, $C = \sin 2\Psi \cos \Delta$, $S = \sin 2\Psi \sin \Delta$) of $(CuS)_{0.64}(ZnS)_{0.36}$ NC thin films were collected *ex situ* at 50° angle of incidence using a single rotating compensator multichannel ellipsometer [46,47] having a spectral range from 0.735 to 5.887 eV (M-2000FI, J. A. Woollam Co.).

2.4. Device fabrication

For the solar cell film stack, CdS (120 nm) and CdTe (3 μm) layers were deposited by commercial vapor transport deposition (VTD) onto TEC™-15 glass substrates by the Willard and Kelsey Solar Group. The CdS/CdTe filmstacks were treated with a saturated $CdCl_2$ solution in methanol at a solution concentration of 2.15 g/100 g of solvent at 20 °C and the devices were annealed at an optimized temperature of 387 °C for 30 min in dry air to advance grain growth, release interfacial strain, and facilitate intermixing at the CdS/ CdTe interface [11,24]. Subsequently, the NC thin films were deposited onto $CdCl_2$-treated CdS/CdTe devices as the HTL. Finally, for some devices, 3 nm Cu and 40 nm Au were thermally evaporated to complete the back contact followed by annealing at 150 °C for 45 min to diffuse the copper. For other devices, the Cu evaporation and annealing steps were omitted. Finally, the

devices were scribed using a 532 nm laser to define an array of approximately 20 cells, each with active device area of 0.08 cm^2.

To prepare the $(CuS)_x(ZnS)_{1-x}$/Cu/ITO back contact, 3 nm Cu was thermally evaporated onto the nanocomposite film followed by annealing at 150 °C for 45 min to diffuse the copper, and subsequently followed by magnetron sputtering of 125 nm of ITO. The ITO was deposited at room temperature at 3 mTorr Ar pressure, and 100 W DC sputtering power. These film stacks were scribed mechanically to produce an array of cells with active device area of 0.08 cm^2.

2.5. Device characterization

Current–voltage (*J V*) characteristics were measured under simulated AM1.5G illumination using a Keithley 2440 digital source meter and a solar simulator (Newport model 91195A-1000). The light intensity of the simulator was calibrated using a standard silicon solar cell obtained from the PV Measurement, Inc. External Quantum Efficiency measurements were performed over a wavelength range of 300–910 nm using a PV Instruments (model IVQE8-C) system.

3. Results and discussion

Fig. 1 shows the SEM images and optical properties of $(CuS)_x(ZnS)_{1-x}$ thin films. The grain size for the $(CuS)_{0.64}(ZnS)_{0.36}$ film as obtained from the SEM images (Fig. 1a) is ~ 10 nm, and these films are more uniform and compact as compared with the $(CuS)_{0.80}(ZnS)_{0.20}$ films (Fig. 1b) which show grain size of ~ 15 nm. Furthermore, the void fraction and surface roughness values extracted from spectroscopic ellipsometry studies concur with SEM images. The stoichiometry of these $(CuS)_x(ZnS)_{1-x}$ films were investigated using EDS analysis. Stoichiometries for both films are spatially uniform within measurement limits as shown in the Supporting information (SI) Fig. S1. The sheet resistances of $(CuS)_{0.64}(ZnS)_{0.36}$ NC and ITO thin films are 2000 Ω/sq and 30 Ω/sq respectively as obtained from 4-point probe measurement. The XRD patterns of Cu-free ZnS films show cubic crystal structure (Fig. S2), and with the addition of CuS, the NC film becomes amorphous, in agreement with results reported previously [36].

Fig. 1(c) presents the transmittance of the NC thin films of thickness ~ 45 nm deposited on bare soda lime glass (SLG), in the 250–850 nm wavelength range. The maximum transmittance of ~ 83% was obtained for the $(CuS)_{0.64}(ZnS)_{0.36}$ film composition at ~ 500 nm wavelength and ~ 82% from the $(CuS)_{0.80}(ZnS)_{0.20}$ film in the same wavelength region. With the increase of ZnS fraction, transmittance does not increase rapidly but as the transparency depends on the crystal size, small crystal size indicates less scattering loss and higher transmittance [48]. In our case, the grain size of the $(CuS)_{0.64}(ZnS)_{0.36}$ is smaller than that of the $(CuS)_{0.80}(ZnS)_{0.20}$. The reflectance spectra of the NC films are shown in Fig. S3(a). ZnS has a direct band gap of 3.7 eV [49] and CuS has a direct band gap about 2.2 eV [50]. Composing the thin film of both CuS and ZnS yields a band gap narrower than ZnS and wider than CuS. Applying Tauc analysis, the band gap energies of $(CuS)_{0.64}(ZnS)_{0.36}$ and $(CuS)_{0.80}(ZnS)_{0.20}$ are found to be 2.70 eV and 2.60 eV respectively (Fig. 1(d)). The relationship between the absorbance and wavelength is shown in Fig. S3(b) (SI). The absorbance increases observed at longer wavelengths arise from free carrier absorption, and the effect is also seen in the absorption coefficient derived from SE as shown in Fig. S4(b).

Determination of the optical response of $(CuS)_{0.64}(ZnS)_{0.36}$ NC thin films, in the form of the energy-dependent complex dielectric function, ($\varepsilon\ (E) = \varepsilon_1\ (E) + i\varepsilon_2\ (E)$) or complex refractive index ($N\ (E) = n\ (E) + ik\ (E) = \varepsilon^{1/2}\ (E)$) spectra, enables assessment of optical and morphological properties relevant to PV and other electronic devices. Spectroscopic reflection, absorption, and transmission of the $(CuS)_{0.64}(ZnS)_{0.36}$ can be determined by using the real and imaginary part of the complex dielectric function. Measurement of the complex dielectric function here indicates contributions from free carrier absorption at low photon energies and critical point electronic transitions at higher photon energies within the optical response. Ellipsometric

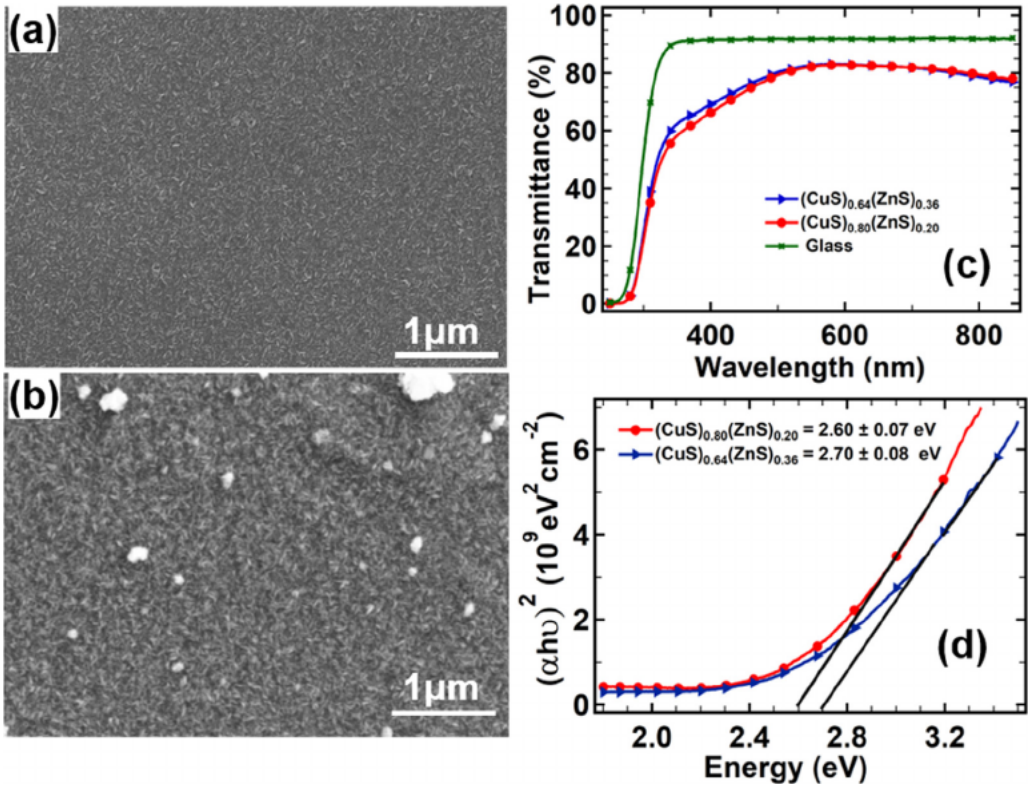

Fig. 1. Scanning electron microscopy (SEM) of (a) $(CuS)_{0.64}(ZnS)_{0.36}$ and (b) $(CuS)_{0.80}(ZnS)_{0.20}$ nanocomposite thin films. (c) transmission spectra and (d) band gap determination via a Tauc plot for $(CuS)_{0.64}(ZnS)_{0.36}$ and $(CuS)_{0.80}(ZnS)_{0.20}$ films.

spectra collected from $(CuS)_{0.64}(ZnS)_{0.36}$ NC films were analyzed using a least square regression analysis and an unweighted error function [51]. Spectra in ε for the bulk film material and the structural parameters, consisting of the surface roughness and bulk layer thickness, are extracted by fitting the experimental ellipsometric spectra to an optical and structural model. This model consists of semi-infinite soda lime glass substrate / NC film / surface roughness / air ambient. Spectra of ε for the film are parameterized by using Lorentz [52], Tauc-Lorentz [53], and Drude oscillators [54]. In addition to the parameters describing spectra in ε, the bulk and surface roughness layer thicknesses (d_b and d_s) are also free parameters in the least squares regression fit. Spectra in ε describing the film surface roughness layer is modeled using a Bruggeman effective medium approximation (EMA) [55,56] consisting of 0.5 of the volume fraction to be identical to the bulk $(CuS)_{0.64}(ZnS)_{0.36}$ layer and the remaining 0.5 volume fraction to be void. The fitted graph is shown in Fig. S4(a) with mean square error 4.6×10^{-3}.

The thicknesses as obtained from the model are $d_b = 25 \pm 3$ nm and $d_s = 16 \pm 4$ nm. Drude oscillator parameters are resistivity ( ) = 0.00142 ± 0.00012 Ω-cm and mean scattering time (τ) = 0.65 ± 0.02 fs. The conductivity of the NC thin film is the reciprocal of resistivity and is found to be 702.2 S-cm^{-1}. Carrier concentration (N) and mobility ( ) can be evaluated from Drude parameters if we know the charge carrier effective mass (m^*). If we assume $m^* = m_e$ for simplicity, we get $N = 3.81 \times 10^{21}$ cm^{-3} and = 1.14 cm^2 / Vs. These electrical transport properties evaluated from the Drude model agree well with those from Hall effect measurements reported in the literature with = 1.5 cm^2 / Vs and $N = 2 \times 10^{21}$ cm^{-3} [33]. Spectra in ε for the NC film for $x = 0.64$ are shown in Fig. 2.

The transmittance spectra of NC films are also calculated using SE (Fig. S5(c)) and the results are very similar to UV/Vis experimental data. The band gap of the $(CuS)_x(ZnS)_{1-x}$ calculated by SE coincides with the band gap calculated by UV/VIS measurements shown in SI as in Fig. S5(d). With these important optoelectronic properties, we come to the conclusion that this material can be used in CdTe thin film solar cells not as an absorber layer because the bandgap is very large, not as a window layer because it is p-type of material, but as a HTL for CdTe devices. The device structures of CdTe solar cells for a standard back contact configuration and with NC HTL are shown in Fig. S6. NC films of different x values were tested with the best results obtained for $x = 0.64$ and 0.80. These results are compared with the Cu/Au standard back contact. At $x = 0.5$ and x = 0.95, the performance of the device decreases as shown in Fig. S7(a).

Fig. 3 displays the device characteristics of the CdTe solar cells with $(CuS)_x(ZnS)_{1-x}$ NC as HTLs. Fig. 3(a) shows the *J-V* curve of highest efficiency cell among 20 cells of each contact type. The solid curves represent measurements under simulated AM1.5G illumination and

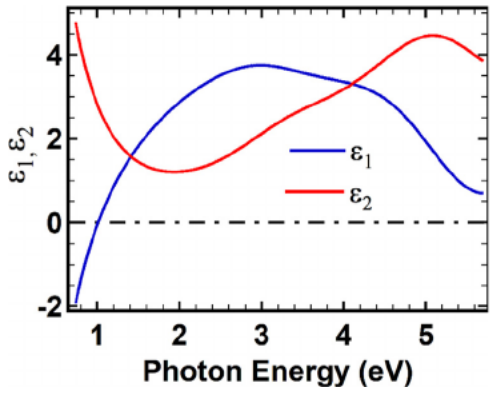

Fig. 2. Real and imaginary parts of the of complex dielectric function, $\varepsilon = \varepsilon_1 + i\varepsilon_2$, as functions of photon energy for thin film $(CuS)_{0.64}(ZnS)_{0.36}$ prepared on soda lime glass.

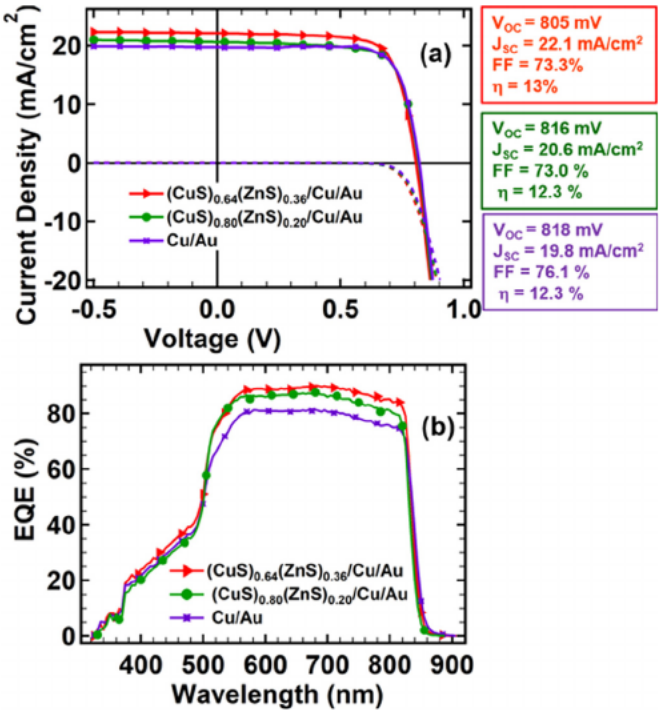

Fig. 3. Performance of CdTe solar cells with and without $(CuS)_x(ZnS)_{1-x}$ NC HTL thin films; these devices include the 3 nm Cu evaporation, as well as post-metallization annealing to diffuse the Cu. (a) Current density and voltage (*J-V*) characteristics under AM1.5G illumination, and (b) external quantum efficiency measurements.

dotted curves represent the dark measurements. Table 1 presents average values for open circuit voltage (V_{OC}), short circuit current density (J_{SC}), fill factor (FF), efficiency ( ), series resistance (R_S), and shunt resistance (R_{Sh}) from 20 cells of the same device for two NC compositions: $(CuS)_{0.64}(ZnS)_{0.36}$, and $(CuS)_{0.80}(ZnS)_{0.20}$, and for the standard Cu/Au contact. The slightly higher series resistance in Table 1 is attributed to the very thin NC film; a thickness dependent study has been performed. The *J-V* characteristics for the NC film thickness dependent study are shown in Fig. S7(b). Since CBD is a self-limiting process due to the final layer thickness being dependent on the bath temperature as well as the concentration of precursors and the pH value, the deposition is done twice to double the thickness [57,58]. From this comparison, we conclude that the thickness of the films used for Fig. 3 and Table 1 are effectively optimized for single layer thickness.

External quantum efficiency (EQE) spectra shown in the Fig. 3(b) show that incorporation of the NC thin film as an HTL in the CdTe solar cell leads to slightly improved current collection in the range of 550–820 nm. The photocurrent collection is low for wavelength below ~540 nm because of parasitic absorption in CdS (120 nm) for which no photocurrent can be collected [24]. The EQE measurement verifies the J_{SC} values obtained from *J-V* measurement. Comparing the two NC compositions as the HTL, $(CuS)_{0.64}(ZnS)_{0.36}$ shows better performance in the current collection than either $(CuS)_{0.80}(ZnS)_{0.20}$ or the Cu/Au back contact. Fig. 3 and Table 1 show that the J_{SC} for devices with $(CuS)_x$ $(ZnS)_{1-x}$ are higher than that of the standard Cu/Au back contact. While it has yet to be determined if this is due to sample-to-sample variation or an improvement at the back contact, this trend persists for samples finished from several locations on the original 2′x4′ coated glass panel.

CuS has p-type conductivity [59] but ZnS typically shows n-type conductivity, [60] and Kudo et al. report that Cu doped ZnS exhibits p-type conductivity [61]. To see the effect of the NC HTL in the absence of Cu, we fabricated solar cells with NC/Au back contacts for $x = 0.64$ and

Table 1
Device performance parameters of 20 CdTe solar cells for different back contact layers (active device area = 0.08 cm^2): average values are expressed along with their standard deviations.

Back contacts	Device parameters					
	V_{OC} (mV)	J_{SC} (mA/cm^2)	*FF* (%)	PCE (%)	R_S (Ω cm^2)	R_{Sh} (Ω cm^2)
$(CuS)_{0.64}(ZnS)_{0.36}$/Cu/Au	803 ± 4	21.6 ± 0.1	72.7 ± 0.8	12.6 ± 0.2	2.8 ± 0.2	1780 ± 380
$(CuS)_{0.80}(ZnS)_{0.20}$/Cu/Au	811 ± 6	20.1 ± 0.4	72.1 ± 0.8	11.8 ± 0.3	2.7 ± 0.7	1330 ± 360
Cu/Au	816 ± 2	19.7 ± 0.2	75.6 ± 0.8	12.1 ± 0.2	2.5 ± 0.1	2800 ± 930

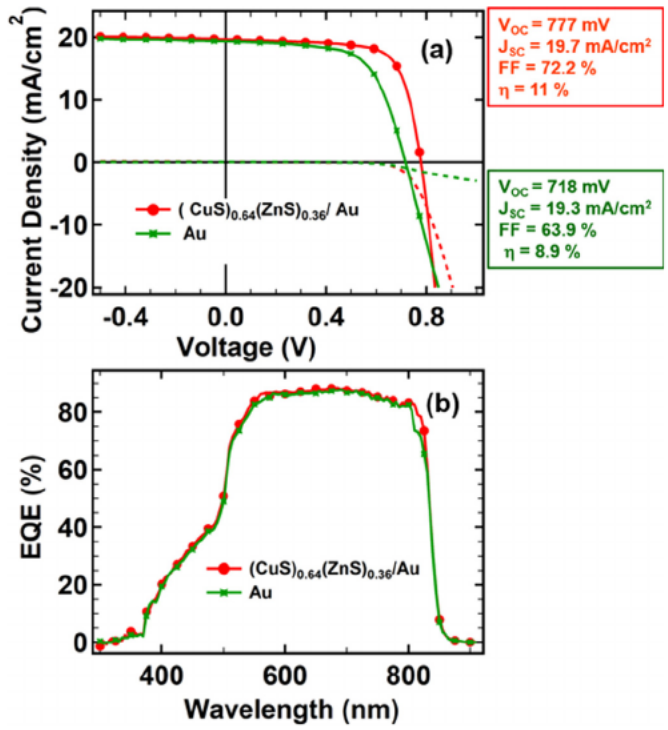

Fig. 4. Performance of CdTe solar cells with and without $(CuS)_{0.64}(ZnS)_{0.36}$ NC thin films as an interface layer; for these devices, the Cu evaporation and post-metallization annealing were omitted. (a) Current density and voltage (*J-V*) characteristics under AM1.5G illumination, and (b) external quantum efficiency (EQE) measurements.

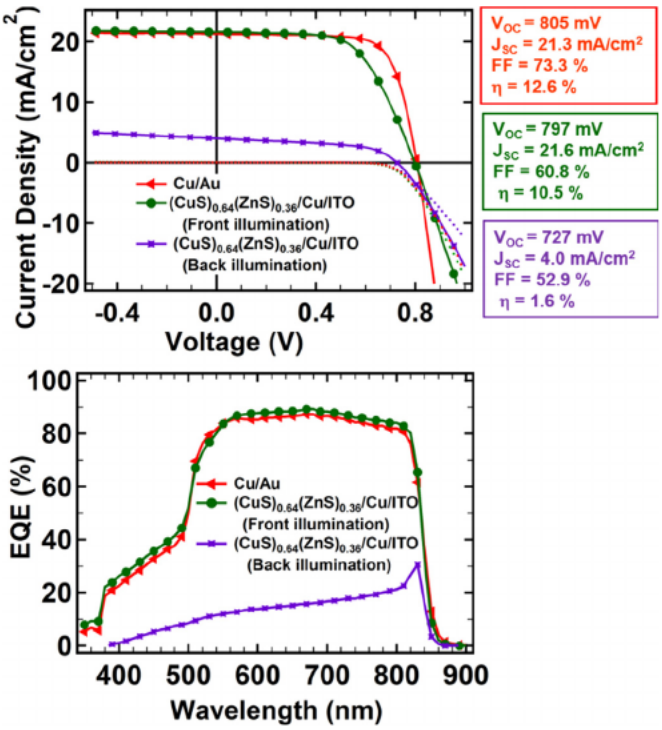

Fig. 5. (a) Current density versus voltage and (b) EQE for $(CuS)_{0.64}(ZnS)_{0.36}$/Cu/ITO back contact in front and back illumination, and Cu/Au back contact in front illumination for CdTe solar cells under the simulated AM1.5G solar irradiance spectrum.

compared the results with Au-only back contacts. Fig. 4(a) shows the *J-V* curves of highest efficiency cell among 15 cells of each contact type measured under simulated AM 1.5G illumination. Table 2 shows the average device parameters with $(CuS)_{0.64}(ZnS)_{0.36}$ /Au, and Au back contacts respectively. The dark *J-V* characteristic shows non-ideal diode behavior compared to $(CuS)_{0.64}(ZnS)_{0.36}$ /Au; the roll-over behavior results from the higher Schottky barrier created by the CdTe/Au interface [62]. From the *J-V* results (Fig. 4(a) and Table 2) we can see that V_{OC} is improved from 718 mV to 777 mV (8.2%), *FF* is improved from 63.9% to 72.2%, and J_{SC} is increased from 19.3 mA/cm^2 to 19.7 mA/cm^2 (2.1%). EQE spectra as shown in Fig. 4(b) confirm the increased J_{SC} from the introduction of the NC HTL films when compared to the Au only back contact. A slight EQE improvement is again seen in the 530 – 820 nm wavelength range.

Determination of the UV–Vis–NIR absorption properties, by both transmission spectroscopy as well as by SE, showed that the NC thin film has high transmittance in the visible region (> 70%). This suggests that it can serve as a transparent back contact layer for use either within a tandem device using CdTe as the top absorber or within a bifacial cell design that enables collection of carriers generated by illumination from the front and back simultaneously. Bifacial devices require a transparent back contact, and we tested this approach by preparing devices with the CdTe/NC/Cu/ITO configuration. Fig. 5 shows the *J-V* characteristics and EQEs of the devices illuminated from both sides. For the front side illumination, the best device showed V_{OC} = 797 mV, J_{SC} = 21.6 mA/cm^2, *FF* = 60.8%, efficiency = 10.5%, and R_S = 10 Ω cm^2. The *FF* is lower than that of the standard Cu/Au back

Table 2
Device parameters of the average ± standard deviation of 15 cells when $(CuS)_{0.64}(ZnS)_{0.36}$/Au and Au were used as back contacts.

Back contacts	Device parameters					
	V_{OC} (mV)	J_{SC} (mA/cm^2)	*FF* (%)	PCE (%)	R_S (Ω cm^2)	R_{Sh} (Ω cm^2)
$(CuS)_{0.64}(ZnS)_{0.36}$/Au	761 ± 12	19.9 ± 0.1	69.7 ± 2.7	10.5 ± 0.7	3.0 ± 0.8	1050 ± 140
Au	693 ± 11	19.2 ± 0.5	56.1 ± 5.2	7.5 ± 0.9	8.9 ± 6	910 ± 200

Table 3
The average device parameters of CdTe solar cells for Cu/Au and $(CuS)_{0.64}(ZnS)_{0.36}$/Cu/ITO as a back contact in both front and back side illuminations. Each tested device has area 0.08 cm^2.

Back contacts	Device parameters					
	V_{OC} (mV)	J_{SC} (mA/cm^2)	*FF* (%)	PCE (%)	R_S (Ω cm^2)	R_{Sh} (Ω cm^2)
Cu/Au (front illumination)	800 ± 5	21.2 ± 1.2	72.2 ± 2.4	12.3 ± 0.6	3.8 ± 0.6	4480 ± 1390
$(CuS)_{0.64}(ZnS)_{0.36}$/Cu/ITO (front illumination)	774 ± 30	23.0 ± 2.2	54.9 ± 4.3	9.2 ± 1.4	10 ± 2.2	1550 ± 940
$(CuS)_{0.64}(ZnS)_{0.36}$/Cu/ITO (back illumination)	721 ± 8	3.8 ± 0.3	49.9 ± 2.5	1.4 ± 0.2	32.3 ± 8.6	510 ± 130

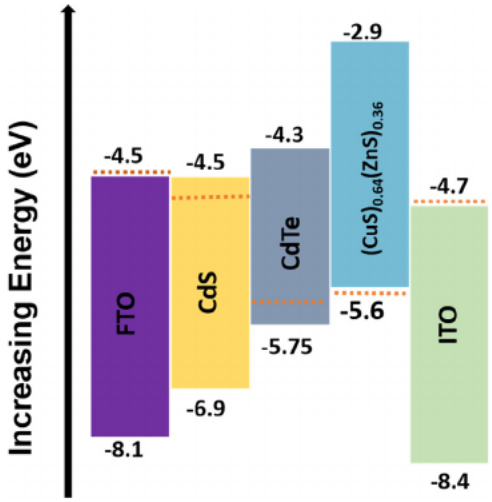

Fig. 6. Non-equilibrium schematic band diagram showing the position of valence band and conduction band edges with respect to the vacuum level for the CdS/CdTe solar cell with $(CuS)_{0.64}(ZnS)_{0.36}$ as an interface layer between CdTe and ITO.

contact, owing to the higher series resistance introduced by the thin HTL and ITO. The device parameters are presented in Table 3. The *Jsc* measured here is confirmed by the EQE measurements as shown in the Fig. 5(b). While analyzing Fig. 5(b), we see that the EQE is greater than 80% with very low variation in the 540–840 nm wavelength range in the superstrate configuration whereas in substrate configuration (back-illumination), the EQE is steadily increasing with wavelength but very poor in the same wavelength range. When the device is illuminated in substrate configuration, photo generated electrons must travel a longer distance to be collected in the front electrode and during this time, collection probability is severely affected by recombination loss due to the low diffusion length in CdTe and the absence of an electric field over the back portion of the CdTe layer.

We modeled our CdTe device structure as glass/FTO/CdS/CdTe/$(CuS)_{0.64}$ $(ZnS)_{0.36}$/ITO in SCAPS [63] software, and the relationship between the carrier density and the thickness of the CdTe was studied from front and back surface illumination. All the simulation parameters used here are borrowed from Phillips et al.'s work except SWNT [26], and the $(CuS)_{0.64}(ZnS)_{0.36}$ parameters were taken from the SE analysis reported here. The free carrier density as a function of distance (μm) profile is shown in Fig. S8(a). The nature of the modeled EQE curve as in Fig. S8(b) from back side illumination matches with our

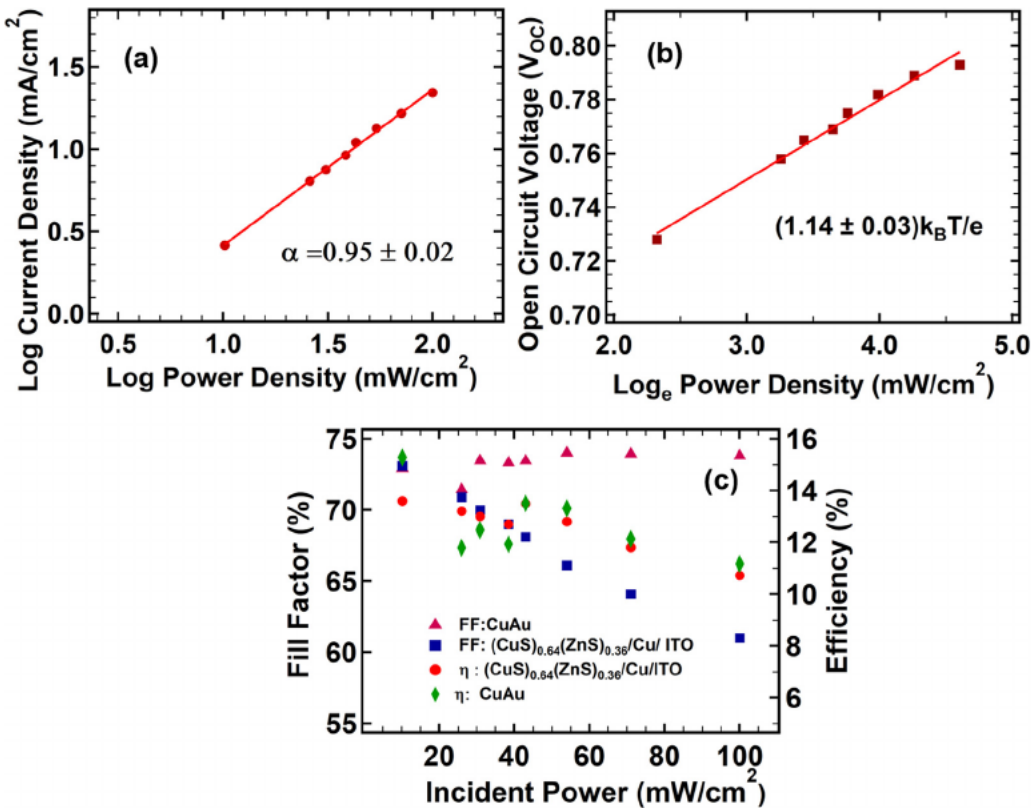

Fig. 7. Light intensity dependent relation: (a) J_{SC} versus incident power (b)V_{OC} versus incident power (c) The variation of *FF* and efficiency of CdTe solar cells having $(CuS)_x(ZnS)_{1-x}$/Cu/ITO back contact and Cu/Au back contact at different intensities of illumination light for front-illumination.

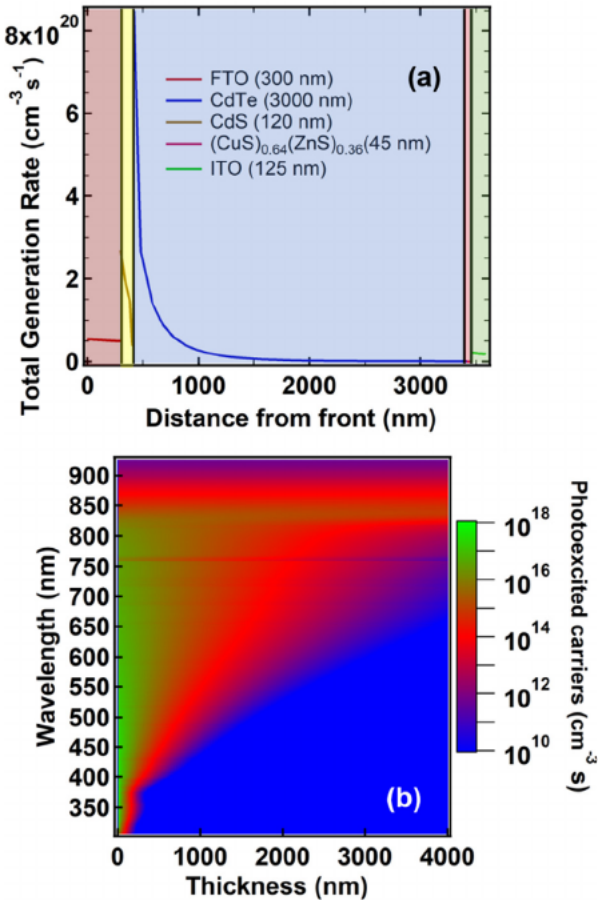

Fig. 8. (a) Calculation of total charge carrier generation rate as a function of distance (nm) from the front contact for the CdTe solar cell. (b) Absorption of photons of different wavelengths and corresponding carrier generations as a function of absorber layer thickness.

experimental result. The modeled curve indicates the photo generated current collection is observed only in the depletion region between the CdTe and CdS.

Furthermore, to analyze the device performance for front illumination and back illumination, a non-equilibrium band diagram has been presented (Fig. 6). Xu et al. reported XPS/UPS measurements for $x = 0.64$ and 0.80, where the CuS fraction dominates, and these composite films behave as p-type degenerate semiconductors for which the valance band edge energies for the $(CuS)_{0.65}(ZnS)_{0.35}$ and $(CuS)_{0.85}(ZnS)_{0.15}$ are 0.4 eV and 0.5 eV above the Fermi level, respectively. Our $(CuS)_{0.64}(ZnS)_{0.36}$ nanocomposite film has composition very close to $(CuS)_{0.65}(ZnS)_{0.35}$ fabricated by Xu et al., and we therefore assume that the valence band maximum of $(CuS)_{0.64}(ZnS)_{0.36}$ remains at ~ 0.5 eV with respect to Fermi level [33]. The postulated band diagram of the CdTe device is shown in Fig. 6. Here, $(CuS)_{0.65}(ZnS)_{0.35}$ acts as an interface layer between the CdTe and ITO. When illuminated from the front side, the carriers photogenerated primarily within the depletion region formed by the junction between the CdS and CdTe. The device efficiency is very low when back-illuminated (through the ITO) due to the lack of a charge-separating electric field near the back contact. When ITO is used as a back contact layer, tunneling is the probable mechanism for hole transfer between the $(CuS)_{0.64}(ZnS)_{0.36}$ and ITO, which is common at the junction between p^+ and n^+ semiconductors [6]. The heavy doping creates a narrow depletion region with a thin barrier which facilitates tunneling of the hole through the $(CuS)_{0.64}(ZnS)_{0.36}$ NC layers into the ITO [64,65].

To understand the different recombination mechanisms, the light intensity dependent *J-V* measurements were performed for $(CuS)_{0.64}(ZnS)_{0.36}$/Cu/ITO back contact devices in the front illumination configuration. This measurement was done at room temperature. The power law relationship between J_{SC} and incident power was analyzed as shown in Fig. 7(a) yielding $\alpha = 0.95 \pm 0.02$. This value indicates efficient charge transfer into the solar cell [66]. The slope of the line (1.14 ± 0.03) $k_B T/e$ was obtained from the natural logarithmic relation between the incident power and V_{OC} shown in Fig. 7(b). This behavior implies that Shockley-Read-Hall recombination is dominant [67,68] and is consistent with increased *FF* for decreasing illumination intensity. The increases in *FF* and efficiency of the solar cells at low light intensity are shown in Fig. 7(c). The qualitative variation of V_{OC} and J_{SC} with respect to the intensity of incident light is shown in Fig. S9 and quantitative variation of V_{OC}, J_{SC}, *FF*, percentage of conversion efficiency (PCE), R_S, and R_{Sh} with respect to the intensity of light is shown in Table S1(SI) when $(CuS)_{0.64}(ZnS)_{0.36}$/ Cu/ ITO was used as a back contact.

For a semiconductor, the absorption coefficient $\alpha(\lambda)$ describes incident light attenuation as photons convert to electron-hole pairs. For a multi-layer CdTe solar cell with the device structure of glass/ FTO (300 nm)/CdS (120 nm)/CdTe (3000 nm)/$(CuS)_{0.64}(ZnS)_{0.36}$ (45 nm)/ ITO (200 nm), Fig. 8(a) illustrates the spectrally-integrated photo generation rate at different layers, for AM1.5G illumination. For the simulation work as shown in Fig. 8, all of the optical parameters were taken from Ref. [69] and optical properties of $(CuS)_{0.64}(ZnS)_{0.36}$ were taken from SE data. The photogeneration rate is very high within the absorber CdTe layer in comparison to the other layers. The spectrally-differentiated absorption of light with respect to the ~ 3 μm thickness of CdTe absorber layer and the corresponding carrier generation were modeled with results shown in Fig. 8(b). This calculation pertains to a bare CdTe layer and omits the glass/FTO/CdS layers. From Fig. 8, it is clear that for most of the supra-bandgap wavelengths, photons are essentially fully absorbed within 1 μm distance except for some of the photons generated within the 800–850 nm wavelength range. Fig. 8(b) demonstrates that, in the case of back side illumination, only the longer wavelength photons generate carriers in the depletion region. Since the diffusion length of the CdTe is ~ 1 μm [70] and the depletion width is also ~ 1 μm [71], charge separation relies heavily on the electric field within the depletion zone. Photo-electrons generated near the back contact must travel a long distance to reach the depletion region and the probability of recombination loss of these electrons remains high. Therefore, the decreases in J_{SC} are shown to agree for the cases of the experimental measurement and simulated EQE. In Fig. 8(b), the artifact near 760 nm is due to the atmospheric absorption line due to oxygen and ozone as included within the AM1.5G standard spectrum.

4. Conclusion

We have achieved a high degree of control over the stoichiometry to prepare highly conductive $(CuS)_x(ZnS)_{1-x}$ NC thin films with high carrier concentration using a cost-effective, solution-based deposition approach at 80 °C. These $(CuS)_x(ZnS)_{1-x}$ NC thin films have a high transmittance (> 70% at visible region), and high band gap energy (~ 2.7 eV) with p-type conductivity. The test of $(CuS)_x(ZnS)_{1-x}$ composite films as the back contact interface layer in CdTe solar cells shows relative device performance enhanced by ~ 3.2% in comparison to the standard Cu/Au back contact and ~ 23.6% in comparison to the Au back contact. Our study indicates that employing the NC thin film HTL reduces recombination loss at the CdTe back contact and increases J_{SC} and ultimately overall efficiency of the devices. Due to their high band gap and high transmittance, these materials are of interest for use in bifacial solar cells. A novel configuration of CdTe/CdS solar cells were demonstrated using the highly transparent $(CuS)_x(ZnS)_{1-x}$ NC thin film as an interface layer and ITO as a transparent back contact. The ITO back contact performed well in front illumination but comparatively lower J_{SC} was obtained in back illumination due to the effective absence of a back-contact depletion region. A successful demonstration using

these nanocomposites as the back contact HTL in CdTe solar cells may also lead to new applications of these materials in other thin film PV devices like tandem cell designs, building-integrated PV, and bifacial solar cells.

Acknowledgements

The authors gratefully acknowledge funding support from the United States Air Force Research Laboratory, Space Vehicles Directorate (Contract# FA9453-11-C-0253), and from the National Science Foundation's Sustainable Energy Pathways Program under Grant CHE-1230246. We would like to thank Willard and Kelsey Solar Group for providing the CdS/CdTe film stacks.

Appendix A. Supporting information

Supplementary data associated with this article can be found in the online version at http://dx.doi.org/10.1016/j.solmat.2018.06.025.

References

[1] V. Tyagi, N.A. Rkkkahim, N. Rahim, A. Jeyraj, L. Selvaraj, Progress in solar PV technology: research and achievement, Renew. Sustain. Energy Rev. 20 (2013) 443–461.
[2] K.P. Bhandari, J.M. Collier, R.J. Ellingson, D.S. Apul, Energy payback time (EPBT) and energy return on energy invested (EROI) of solar photovoltaic systems: a systematic review and meta-analysis, Renew. Sustain. Energy Rev. 47 (2015) 133–141.
[3] M.A. Green, Y. Hishikawa, E.D. Dunlop, D.H. Levi, J. Hohl-Ebinger, A.W.Y. Ho-Baillie, Solar cell efficiency tables (version 51), Prog. Photovolt.: Res. Appl. 26 (2018) 3–12.
[4] A. Cannavale, G.E. Eperon, P. Cossari, A. Abate, H.J. Snaith, G. Gigli, Perovskite photovoltachromic cells for building integration, Energy Environ. Sci. 8 (2015) 1578–1584.
[5] A. Luque, J. Ruiz, A. Cuevas, J. Eguren, M. Agost, Double sided/DS/solar cells to improve static concentration, in: Proceedings of Photovoltaic Solar Energy Conference, 1978, pp. 269–277.
[6] A.N. Tiwari, G. Khrypunov, F. Kurdzesau, D. Bätzner, A. Romeo, H. Zogg, CdTe solar cell in a novel configuration, Prog. Photovolt.: Res. Appl. 12 (2004) 33–38.
[7] R.R. Khanal, A.B. Phillips, Z. Song, Y. Xie, H.P. Mahabaduge, M.D. Dorogi, S. Zafar, G.T. Faykosh, M.J. Heben, Substrate configuration, bifacial CdTe solar cells grown directly on transparent single wall carbon nanotube back contacts, Sol. Energy Mater. Sol. Cells 157 (2016) 35–41.
[8] A. Cuevas, A. Luque, J. Eguren, J. Del Alamo, 50 Per cent more output power from an albedo-collecting flat panel using bifacial solar cells, Sol. Energy 29 (1982) 419–420.
[9] S. Ito, S.M. Zakeeruddin, P. Comte, P. Liska, D. Kuang, M. Grätzel, Bifacial dye-sensitized solar cells based on an ionic liquid electrolyte, Nat. Photonics 2 (2008) 693.
[10] T.T. Chow, A review on photovoltaic/thermal hybrid solar technology, Appl. Energy 87 (2010) 365–379.
[11] K.V. Krishna, V. Dutta, Effect of in situ $CdCl_2$ treatment on spray deposited CdTe CdS heterostructure, J. Appl. Phys. 96 (2004) 3962–3971.
[12] S. Chander, M. Dhaka, Time evolution to $CdCl_2$ treatment on Cd-based solar cell devices fabricated by vapor evaporation, Sol. Energy 150 (2017) 577–583.
[13] Z. Fang, X.C. Wang, H.C. Wu, C.Z. Zhao, Achievements and challenges of CdS/CdTe solar cells, Int. J. Photoenergy 2011 (2011).
[14] A.C. Tamboli, D.C. Bobela, A. Kanevce, T. Remo, K. Alberi, M. Woodhouse, Low-cost CdTe/silicon tandem solar cells, IEEE J. Photovolt. 7 (2017) 1767–1772.
[15] J. Freeouf, J. Woodall, Schottky barriers: an effective work function model, Electronic Structure of Metal-Semiconductor Contacts, Springer, 1990, pp. 154–156.
[16] R.K. Swank, Surface Properties of II-VI Compounds, Phys. Rev. 153 (1967) 844–849.
[17] B.E. McCandless, J.R. Sites, Cadmium telluride solar cells, Handbook of Photovoltaic Science and Engineering 2 (2003).
[18] D. Rioux, D.W. Niles, H. Höchst, ZnTe: a potential interlayer to form low resistance back contacts in CdS/CdTe solar cells, J. Appl. Phys. 73 (1993) 8381–8385.
[19] H. Kawazoe, H. Yanagi, K. Ueda, H. Hosono, Transparent p-type conducting oxides: design and fabrication of pn heterojunctions, MRS Bull. 25 (2000) 28–36.
[20] A. Banerjee, K. Chattopadhyay, Recent developments in the emerging field of crystalline p-type transparent conducting oxide thin films, Prog. Cryst. Growth Charact. Mater. 50 (2005) 52–105.
[21] H. Chou, A. Rohatgi, E. Thomas, S. Kamra, A. Bhat, Effects of Cu on CdTe/CdS heterojunction solar cells with Au/Cu contacts, J. Electrochem. Soc. 142 (1995) 254–259.
[22] T. Gessert, A. Mason, P. Sheldon, A. Swartzlander, D. Niles, T. Coutts, Development of Cu-doped ZnTe as a back-contact interface layer for thin-film CdS/CdTe solar cells, J. Vac. Sci. Technol. A: Vac. Surf. Films 14 (1996) 806–812.
[23] J.H. Yun, K.H. Kim, D.Y. Lee, B.T. Ahn, Back contact formation using Cu_2Te as a Cu-doping source and as an electrode in CdTe solar cells, Sol. Energy Mater. Sol. Cells 75 (2003) 203–210.
[24] K.P. Bhandari, P. Koirala, N.R. Paudel, R.R. Khanal, A.B. Phillips, Y. Yan, R.W. Collins, M.J. Heben, R.J. Ellingson, Iron pyrite nanocrystal film serves as a copper-free back contact for polycrystalline CdTe thin film solar cells, Sol. Energy Mater. Sol. Cells 140 (2015) 108–114.
[25] E. Bastola, K.P. Bhandari, R.J. Ellingson, Application of composition controlled nickel-alloyed iron sulfide pyrite nanocrystal thin films as the hole transport layer in cadmium telluride solar cells, J. Mater. Chem. C 5 (2017) 4996–5004.
[26] A.B. Phillips, R.R. Khanal, Z. Song, R.M. Zartman, J.L. DeWitt, J.M. Stone, P.J. Roland, V.V. Plotnikov, C.W. Carter, J.M. Stayancho, Wiring-up carbon single wall nanotubes to polycrystalline inorganic semiconductor thin films: low-barrier, copper-free back contact to CdTe solar cells, Nano Lett. 13 (2013) 5224–5232.
[27] A.L. Fahrenbruch, Ohmic contacts and doping of CdTe, Sol. Cells 21 (1987) 399–412.
[28] S. Demtsu, J. Sites, Effect of back-contact barrier on thin-film CdTe solar cells, Thin Solid Films 510 (2006) 320–324.
[29] N. Strevel, L. Trippel, C. Kotarba, I. Khan, Improvements in CdTe module reliability and long-term degradation through advances in construction and device innovation, Photovolt. Int. 22 (2013) 66–74.
[30] J. Sites, J. Pan, Strategies to increase CdTe solar-cell voltage, Thin Solid Films 515 (2007) 6099–6102.
[31] A. Romeo, M. Terheggen, D. Abou-Ras, D. Bätzner, F.J. Haug, M. Kälin, D. Rudmann, A. Tiwari, Development of thin-film Cu (In, Ga) Se_2 and CdTe solar cells, Prog. Photovolt.: Res. Appl. 12 (2004) 93–111.
[32] L. Ma, S. Ma, H. Chen, X. Ai, X. Huang, Microstructures and optical properties of Cu-doped ZnO films prepared by radio frequency reactive magnetron sputtering, Appl. Surf. Sci. 257 (2011) 10036–10041.
[33] X. Xu, J. Bullock, L.T. Schelhas, E.Z. Stutz, J.J. Fonseca, M. Hettick, V.L. Pool, K.F. Tai, M.F. Toney, X. Fang, Chemical bath deposition of p-type transparent, highly conducting $(CuS)_x(ZnS)_{1-x}$ nanocomposite thin films and fabrication of Si heterojunction solar cells, Nano Lett. 16 (2016) 1925–1932.
[34] N. Romeo, A. Bosio, R. Tedeschi, A. Romeo, V. Canevari, A highly efficient and stable CdTe/CdS thin film solar cell, Sol. Energy Mater. Sol. Cells 58 (1999) 209–218.
[35] B.E. McCandless, K.D. Dobson, Processing options for CdTe thin film solar cells, Sol. Energy 77 (2004) 839–856.
[36] D.E. Ortíz-Ramos, L.A. González, R. Ramirez-Bon, p-Type transparent Cu doped ZnS thin films by the chemical bath deposition method, Mater. Lett. 124 (2014) 267–270.
[37] K. Yang, M. Ichimura, Fabrication of transparent p-Type Cu_xZn_yS thin films by the electrochemical deposition method, Jpn. J. Appl. Phys. 50 (2011) 040202.
[38] M. Dula, K. Yang, M. Ichimura, Photochemical deposition of a p-type transparent alloy semiconductor Cu_xZn_yS, Semicond. Sci. Technol. 27 (2012) 125007.
[39] L. Ma, X. Ai, X. Wu, Effect of substrate and Zn doping on the structural, optical and electrical properties of CdS thin films prepared by CBD method, J. Alloy. Compd. 691 (2017) 399–406.
[40] J.J. Becker, X. Xu, R. Woods-Robinson, C.M. Campbell, M. Lassise, J. Ager, Y. Zhan CuZnS, hole contacts on monocrystalline CdTe solar cells, in: Proceedings of the 44th IEEE Photovoltaic Specialists Conference, 2017.
[41] K. Khanal Subedi, K.P. Bhandari, E. Bastola, R.J. Ellingson, 13% CdS/CdTe solar cell using a nanocomposite $(CuS)_x(ZnS)_{1-x}$ thin film hole transport layer, in: Proceedings of the 44th IEEE PVSC Conference- Washington, DC, 2017.
[42] E. Bastola, K.K. Subedi, K.P. Bhandari, R.J. Ellingson, Solution-processed nanocrystal based thin films as hole transport materials in cadmium telluride photovoltaics, MRS Adv. (2018) 1–7.
[43] T. Schneller, R. Waser, M. Kosec, D. Payne, Chemical Solution Deposition of FFunctional Oxide Thin Films, Springer, 2013.
[44] H. Zhang, X. Ma, D. Yang, Effects of complexing agent on CdS thin films prepared by chemical bath deposition, Mater. Lett. 58 (2004) 5–9.
[45] M. Gharabaghi, M. Irannajad, A.R. Azadmehr, Selective sulphide precipitation of heavy metals from acidic polymetallic aqueous solution by thioacetamide, Ind. Eng. Chem. Res. 51 (2012) 954–963.
[46] J. Lee, P. Rovira, I. An, R. Collins, Rotating-compensator multichannel ellipsometry: applications for real time Stokes vector spectroscopy of thin film growth, Rev. Sci. Instrum. 69 (1998) 1800–1810.
[47] B.D. Johs, J.A. Woollam, C.M. Herzinger, J.N. Hilfiker, R.A. Synowicki, C.L. Bungay, Overview of variable-angle spectroscopic ellipsometry (VASE): II. Advanced applications, Opt. Metrol. (1999) 29–58.
[48] Y. Lu, X. Meng, G. Yi, J. Jia, In situ growth of CuS thin films on functionalized self-assembled monolayers using chemical bath deposition, J. Colloid Interface Sci. 356 (2011) 726–733.
[49] A. Goudarzi, G.M. Aval, R. Sahraei, H. Ahmadpoor, Ammonia-free chemical bath deposition of nanocrystalline ZnS thin film buffer layer for solar cells, Thin Solid Films 516 (2008) 4953–4957.
[50] C. Na cu, I. Pop, V. Ionescu, E. Indrea, I. Bratu, Spray pyrolysis deposition of CuS thin films, Mater. Lett. 32 (1997) 73–77.
[51] B. Johs, C. Herzinger, Quantifying the accuracy of ellipsometer systems, Phys. Status Solidi (C) 5 (2008) 1031–1035.
[52] H. Tompkins, E.A. Irene, Handbook of Ellipsometry, William Andrew, 2005.
[53] G. Jellison Jr, F. Modine, Parameterization of the optical functions of amorphous materials in the interband region, Appl. Phys. Lett. 69 (1996) 371–373.
[54] T.E. Tiwald, D.W. Thompson, J.A. Woollam, W. Paulson, R. Hance, Application of IR variable angle spectroscopic ellipsometry to the determination of free carrier concentration depth profiles, Thin Solid Films 313 (1998) 661–666.
[55] D. Aspnes, J. Theeten, F. Hottier, Investigation of effective-medium models of

microscopic surface roughness by spectroscopic ellipsometry, Phys. Rev. B 20 (1979) 3292.
[56] I. Subedi, K.P. Bhandari, R.J. Ellingson, N.J. Podraza, Near infrared to ultraviolet optical properties of bulk single crystal and nanocrystal thin film iron pyrite, Nanotechnology 27 (2016) 295702.
[57] P. Vas-Umnuay, C.-h. Chang, Growth kinetics of copper sulfide thin films by chemical bath deposition, ECS J. Solid State Sci. Technol. 2 (2013) P120–P129.
[58] M. Ortega-López, A. Avila-Garc´, M. Albor-Aguilera, V.S. Resendiz, Improved efficiency of the chemical bath deposition method during growth of ZnO thin filmsImproved efficiency of the chemical bath deposition method during growth of ZnO thin films, Mater. Res. Bull. 38 (2003) 1241–1248.
[59] W. Liang, M.-H. Whangbo, Conductivity anisotropy and structural phase transition in covellite CuS, Solid State Commun. 85 (1993) 405–408.
[60] X. Ma, Study of the P-type doping properties of ZnS nanocrystals, J. Nanomater. 2011 (2011) 37.
[61] A. Kudo, M. Sekizawa, Photocatalytic H_2 evolution under visible light irradiation on Zn_{1-x} Cu_x S solid solution, Catal. Lett. 58 (1999) 241–243.
[62] A. Niemegeers, M. Burgelman, Effects of the Au/CdTe back contact on IV and CV characteristics of Au/CdTe/CdS/TCO solar cells, J. Appl. Phys. 81 (1997) 2881–2886.
[63] M. Burgelman, P. Nollet, S. Degrave, Modelling polycrystalline semiconductor solar cells, Thin Solid Films 361 (2000) 527–532.
[64] J. Zide, A. Kleiman-Shwarsctein, N. Strandwitz, J. Zimmerman, T. Steenblock-Smith, A. Gossard, A. Forman, A. Ivanovskaya, G. Stucky, Increased efficiency in multijunction solar cells through the incorporation of semimetallic ErAs nanoparticles into the tunnel junction, Appl. Phys. Lett. 88 (2006) 162103.
[65] B. Yu, F. Zhu, H. Wang, G. Li, D. Yan, All-organic tunnel junctions as connecting units in tandem organic solar cell, J. Appl. Phys. 104 (2008) 114503.
[66] D. Bi, L. Yang, G. Boschloo, A. Hagfeldt, E.M. Johansson, Effect of different hole transport materials on recombination in $CH_3NH_3PbI_3$ perovskite-sensitized mesoscopic solar cells, J. Phys. Chem. Lett. 4 (2013) 1532–1536.
[67] S.R. Cowan, W.L. Leong, N. Banerji, G. Dennler, A.J. Heeger, Identifying a threshold impurity level for organic solar cells: enhanced first-order recombination via well-defined PC84BM traps in organic bulk heterojunction solar cells, Adv. Funct. Mater. 21 (2011) 3083–3092.
[68] W. Shockley, W. Read Jr, Statistics of the recombinations of holes and electrons, Phys. Rev. 87 (1952) 835.
[69] P. Koirala, J. Li, H.P. Yoon, P. Aryal, S. Marsillac, A.A. Rockett, N.J. Podraza, R.W. Collins, Through-the-glass spectroscopic ellipsometry for analysis of CdTe thin-film solar cells in the superstrate configuration, Prog. Photovolt.: Res. Appl. 24 (2016) 1055–1067.
[70] M.J. Romero, T.A. Gessert, M.M. Al-Jassim, Carrier diffusion and radiative recombination in CdTe thin films, Appl. Phys. Lett. 81 (2002) 3161–3163.
[71] U. Jahn, T. Okamoto, A. Yamada, M. Konagai, Doping and intermixing in CdS/CdTe solar cells fabricated under different conditions, J. Appl. Phys. 90 (2001) 2553–2558.